Metal Hydrides-Based Hydrogen Storage for Light Mobility Applications: Performance Assessment through 1D Numerical Modeling

Journal of Physics: Conference Series **3143** (2025) 012076 doi:10.1088/1742-6596/3143/1/012076

Metal Hydrides-Based Hydrogen Storage for Light Mobility Applications: Performance Assessment through 1D Numerical Modeling

Lorenzo **Bartolucci[1], *Edoardo* Cennamo[1*], *Stefano* Cordiner[1], *Vesselin K.* Krastev[2], *Vincenzo* Mulone[1], *Alessandro* Polimeni[1]**

[1] Department of Industrial Engineering, Tor Vergata University of Rome, via del Politecnico 1, 00133, Rome, Italy
[2] Enterprise Engineering Department, Tor Vergata University of Rome, via del Politecnico 1, 00133, Rome, Italy

[*]E-mail: edoardo.cennamo@uniroma2.it

Abstract. The urgent need to reduce emissions and environmental pollutants requires a substantial diversification of mobility solutions and energy sources. Hydrogen is increasingly recognized as a key energy carrier due to its potential for zero-emission applications, high energy density and compatibility with renewable energy sources. However, efficient hydrogen storage is still a critical challenge, as conventional methods such as high-pressure tanks still present high energy intensity and safety and logistical concerns. Metal hydrides, composed of metal powder alloys, have emerged as a promising alternative, offering safe and compact storage at moderate pressures, while posing relevant challenges related to their complex thermal management.
This study presents a one-dimensional numerical model to simulate the thermo-fluid dynamic behavior of metal hydride tanks under realistic load conditions. The model was validated against CFD-based literature data on $LaNi_5$ alloys and both absorption and desorption tests confirm its predictive capability for temperature-driven storage dynamics.
The model was then applied to a commercial AB_2-type alloy, integrated into a light-duty hydrogen storage tank. A set of simulations was conducted to assess its performance in a fuel cell hybrid electric microcar under a WMTC driving cycle. The analysis highlights the limitations of natural convection in sustaining hydrogen delivery over time and demonstrates the benefits of a passive thermal management strategy based on forced convection using the exhaust airflow from the fuel cell stack. This configuration led to a 75% increase in operating time compared to natural convection, significantly enhancing storage autonomy while maintaining low system complexity.
The proposed modeling framework provides a robust tool for supporting the design and integration of metal hydride storage systems in micromobility applications, offering valuable insights into the role of thermal management and seasonal conditions on system performance.

1. Introduction

The global effort to decarbonize the transport sector has spurred interest in innovative energy vectors capable of enabling sustainable mobility [1]. Among the proposed solutions, hydrogen-powered vehicles represent a promising pathway, especially when employing renewable hydrogen (so-called green hydrogen) [2]. In this context, Fuel Cell Hybrid Electric Vehicles (FCHEVs) have attracted considerable attention [3] owing to their appealing characteristics, such as high efficiency, extended drivable range and energy regeneration features.

Moreover, micromobility has emerged as a strategic field for sustainability improvements and economic growth [4]. Indeed, Light Electric Vehicles (LEVs), such as quadricycles, are increasingly considered as viable alternatives in urban environments, thanks to their compact dimensions, limited energy requirements and regulatory advantages. In this domain, FCHEVs could represent an attractive solution to overcome the limitations of battery-only architectures, especially in terms of recharge time, overall autonomy and lack of sufficient infrastructures. For instance, Bartolucci *et al.* in [5, 6] introduced detailed and validated platforms to assess the dynamic operation of hybrid microcars powered by fuel cells (FCs) and a battery pack; the proposed analyses underscore the potential of integrating a hydrogen-based hybrid powertrain in light-weight applications, which has been tested in real-world scenarios.

However, the widespread adoption of hydrogen-powered mobility is still hindered by several challenges, one of which is storage, which significantly impacts both vehicle design and operational safety [7]. Current technologies, such as high-pressure tanks (typically operating at 350–700 bar), require significant energy input for gas compression and impose constraints in terms of structural reinforcement, safety systems and volumetric efficiency. In this framework, solid-state storage using Metal Hydrides (MH) has emerged as a potential alternative, particularly suitable for LEVs and micromobility contexts where compactness is essential. They enable hydrogen storage at moderate pressure levels (below 30 bar), with the additional benefit of reversible absorption and release mechanisms, strongly improving the volumetric energy density [8].

Metal hydrides are solid-state materials capable of absorbing and desorbing hydrogen through reversible thermochemical reactions. Their operational characteristics, however, are tightly coupled with temperature and pressure conditions, making thermal management a critical aspect for their effective use [9]. In particular, the exothermic nature of hydrogen absorption and the endothermic character of desorption require precise control of heat exchange processes to ensure system stability and continuity of hydrogen supply [2]. For this reason, several studies, including those by Bartolucci and Krastev [10], have investigated the integration of metal hydrides with high-efficiency thermal jackets, such as those based on Phase Change Materials (PCM), demonstrating the critical role of buoyancy-driven convection and PCM selection on hydrogen absorption performance.

Several studies have investigated the potential of integrating MH tanks into hydrogen-powered vehicles. Lototskyy *et al.* [11] explored their application in utility vehicles and forklifts, demonstrating the importance of effective thermal coupling to sustain the desorption process. Scarpati *et al.* [12] provided a comprehensive overview of the main materials investigated for mobile storage, identifying AB_2-type alloys as a promising trade-off between storage capacity and operating pressure. A relevant example is the work by Di Giorgio *et al.* [13], which presents the development of a plug-in fuel cell electric scooter featuring a hybrid energy storage system that thermally integrates a lithium battery pack with a metal hydride-based hydrogen tank. This configuration exploits the endothermic desorption of hydrogen for battery thermal management, significantly enhancing the system compactness and energy density.

Guizzi *et al.* [14], focusing on small-scale FC systems, emphasized the need to develop numerical tools capable of accounting for the interaction between thermal and fluid dynamic behavior of hydride-based tanks. Building on these findings, simulation platforms have become

increasingly relevant to support the design and integration of metal hydride systems. Their role is crucial in assessing the thermal response, dynamic behavior and recharge capabilities of hydride tanks under realistic operating conditions.

In this work, a detailed numerical model is developed to simulate the thermofluid dynamics of metal hydride-based storage systems under varying operating conditions, such as load profiles and ambient temperatures. After a preliminary validation against literature data, the model is applied to a commercial AB_2-type alloy in a realistic automotive scenario: an experimental hydrogen flow rate profile, extracted from the simulation of the hybrid microcar through a Hardware-in-the-Loop (HIL) platform [15] is used to operate the analyzed system under real vehicle demands. Moreover, thermal management implications are investigated, assessing the system performance under natural and forced convection, as well as an ideal active cooling. The main goal of the analysis is to prove the feasibility of integrating metal hydride tanks into a fuel cell hybrid electric microcar, considering the implications for range, autonomy and system compactness.

2. Methodology

Developing an accurate model to simulate the absorption and desorption dynamics of a metal hydride storage tank is essential for assessing the technical feasibility and operational effectiveness of this hydrogen storage technology in the context of sustainable mobility. A key factor in this evaluation is the system thermal and pressure stability, which directly influences the alloy ability to store and release hydrogen.

During absorption, the exothermic nature of the reaction can cause a temperature rise that inhibits further hydrogen intake unless adequate heat removal is ensured. Conversely, in the desorption process, the reaction endothermicity may lead to excessive temperature drop, potentially halting hydrogen release if no external heat is supplied.

In this study, a one-dimensional numerical model was implemented in MATLAB/Simulink to represent the thermo-fluid dynamic behavior of metal hydride tanks, considering governing equations, thermophysical parameters and system geometry. The target configuration is based on the MyH2 3000 storage tank by H2planet, which contains an AB_2-type Hydralloy C5 alloy manufactured by Gesellschaft für Elektrometallurgie (GfE) [16, 17]; detailed geometrical and thermodynamic properties are reported in Table 1.

Furthermore, a model validation process was carried out by comparing simulation results against experimental data provided by Jemni *et al.* [18] and numerical data from Chung and Ho [19], who tested a $LaNi_5$-based storage system under controlled conditions.

Table 1. H2planet MyH2 3000 technical specifications.

Property	Symbol	Value
Activation energy for desorption [20]	$E_{a,d}$	12.923 kJ mol^{-1}
Density of hydride alloy (dehydrogenated) [16]	$\rho_{MH,0}$	6300 kg m^{-3}
Density of hydride alloy (fully saturated)	$\rho_{MH,max}$	6416 kg m^{-3}
Hydride alloy type [17]		AB_2
Internal cylinder volume [17]	V_{Tank}	0.00580 m^3
Maximum H_2 charging pressure [17]		30 bar (static)
Maximum operating pressure [17]		30 bar
Maximum operating temperature [17]		65 °C
Minimum cooling temperature during charging [17]		10 °C
Molar mass of hydrogen	M_{MH}	0.1037 kg mol^{-1}
Nominal capacity [17]		270 g_{H2} (3 Nm^3)
Occupied volume by the hydride material	V_{MH}	0.00435 m^3
Porosity	ε	0.5
Pre-exponential factor for desorption [20]	$K_{0,d}$	10.81 s^{-1}
Reaction enthalpy	ΔH_d	-27.83 kJ mol^{-1}
Reaction entropy	ΔS_d	109.90 J mol^{-1} K^{-1}
Specific heat at constant pressure [21]	$C_{p_{MH}}$	0.5 kJ kg^{-1} K^{-1}
Tank diameter [17]	D	15 cm
Tank height [17]	A	53 cm
Thermal conductivity of the metal alloy	k_{MH}	1.5 W m^{-1} K^{-1}
Thermal conductivity of the tank	k_{Tank}	55 W m^{-1} K^{-1}
Total mass of the system [17]		22 kg

2.1. PCI Curves

The thermodynamic behavior of metal hydrides is strongly dependent on the equilibrium conditions defined by the Pressure-Composition-Isotherm (PCI) curves. These curves describe the relationship between the equilibrium hydrogen pressure, the temperature and the Hydrogen-to-Metal ratio (H/M) in the alloy. They are essential for calculating the equilibrium pressure under varying thermal conditions and for estimating the initial hydrogen concentration stored into the system.

PCI curves of Hydralloy C5 were imported from experimental literature data [22] and then interpolated using the third-order rational equation, as proposed by Hariyadi *et al.* in [23]:

$$p_{eq}(C) = \frac{\mathrm{a}_1 C^3 + \mathrm{a}_2 C^2 + \mathrm{a}_3 C + \mathrm{a}_4}{C^3 + \mathrm{a}_5 C^2 + \mathrm{a}_6 C + \mathrm{a}_7} \quad (1)$$

Where p_{eq} is the equilibrium pressure, C is the hydrogen concentration – expressed as the ratio between the mass of absorbed hydrogen and the total mass of the hydride alloy – and $\mathrm{a}_1 \dots \mathrm{a}_7$ are the interpolation coefficients. The result of the interpolation process is reported in Figure 1.

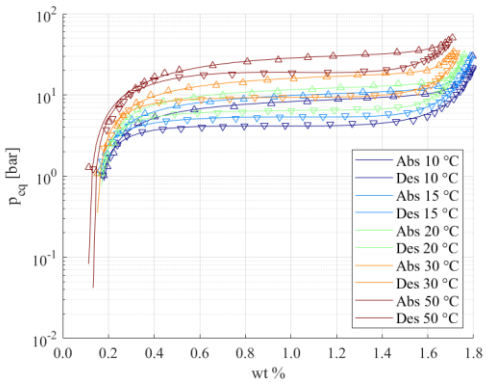

Figure 1. Interpolated PCI curves of Hydralloy C5; triangles indicate experimental data points from [22].

As easily noticeable from the figure, the PCI curve exhibits a characteristic plateau region at fixed temperature, associated with the two-phase equilibrium between the metal and the hydride phase. The slope and length of the plateau provide insights into the material suitability for practical applications, particularly in terms of reversible capacity and operating pressure window.

In this plateau region, for a given metal hydride, the equilibrium pressure follows the van't Hoff equation:

$$\ln\left(\frac{p_{eq}}{p_0}\right) = -\frac{\Delta H_d}{RT} + \frac{\Delta S_d}{R} \tag{2}$$

where T is the absolute temperature, p_0 a reference pressure, ΔH_d the enthalpy of reaction, ΔS_d the entropy of reaction and R the universal gas constant.

In the present work, PCI data were used both to calculate the equilibrium pressure for dynamic simulations and to estimate the initial hydrogen content stored in the tank before the desorption phase. At least two isotherms were used to extract the thermodynamic parameters ΔH_d and ΔS_d of the van't Hoff equation via linear fitting. These values were then employed in the model to dynamically update the equilibrium pressure based on the local temperature within each node of the simulation domain.

2.2. Reaction kinetic

The van't Hoff equation alone is not sufficient to describe the dynamic behavior of hydrogen absorption and desorption processes in metal hydrides. It is then necessary to adopt a kinetic formulation to fully characterize the system; it enables the analysis of the effects of temperature T, pressure p and hydrogenation state of the alloy, typically expressed as the reacted fraction X. According to the recommendations of the ICTAC Kinetics Committee [24], the reaction rate can be described through a separation effect approach, as stated in the following equation:

$$\frac{\partial \mathrm{X}}{\partial t} = k(T)\, f(p)\, f(\mathrm{X}) \tag{3}$$

The pressure-dependent function $f(p)$ accounts for the thermodynamic equilibrium condition and varies according to whether absorption or desorption is being modeled. For the absorption process, according to [23], a commonly used expression in literature is:

$$f(p) = \ln\left(\frac{p}{p_{eq}}\right) \tag{4}$$

where p is the actual hydrogen pressure inside the tank.

The temperature-dependent kinetic term $k(T)$ follows an Arrhenius-type behavior:

$$k(T) = k_0 \exp\left(-\frac{E_a}{RT}\right) \tag{5}$$

where k_0 is the pre-exponential factor and E_a the activation energy of the process.

Finally, the conversion-dependent term $f(\mathrm{X})$, representing the progression of the reaction, can also take different forms depending on the alloy and reaction mechanism. According to [23], a commonly adopted expression is the Johnson-Mehi-Avrami-Kolmogorov one, based on the alpha and beta phase nuclei growth:

$$f(\mathrm{X}) = -(\ln(1-\mathrm{X}))^{\frac{1}{\mathrm{n}}} \tag{6}$$

where n is the value of the exponential, generally ranging from 0.5 to 4, and X is the mass fraction of absorbed hydrogen, defined as:

$$\mathrm{X} = \frac{C - C_{min}}{C_{max} - C_{min}} \tag{7}$$

with C being the hydrogen content in the alloy.

2.3. Reaction dynamic

The transient evolution of the system can be described through the conservation equations of mass and energy. In accordance with the assumptions reported by Brown *et al.* [21], the temperature of the gas phase is considered equal to that of the solid hydride. Therefore, the energy balance for the gas can be neglected and only the thermal evolution of the solid phase is considered. Conversely, mass balance is applied to both solid and gaseous phases.

The mass conservation equation for hydrogen in the gas phase is expressed as:

$$V_g \frac{\mathrm{d}\rho_g}{\mathrm{d}t} + \nabla \cdot (\rho_g v_g) = -n_d V_g \pm \frac{\dot{m}_{H_2}}{V_g} \tag{8}$$

where V_g is the gas volume, ρ_g is the gas density, v_g is the gas velocity vector due to internal pressure gradients, $\dot{m}_{H_2}$ is the hydrogen mass flow entering or exiting the tank and n_d is the reaction rate per unit volume for desorption.

The gas velocity is described by Darcy's law:

$$v_g = -\frac{K}{\mu}\nabla p \tag{9}$$

where K is the permeability of the hydride bed and μ the dynamic viscosity of hydrogen.

The reaction rate n_d is expressed as:

$$n_d = k(T)\, k(p)\, (\rho_{MH} - \rho_{MH,0}) \tag{10}$$

where $\rho_{MH,0}$ represents the hydride density when fully depleted, while ρ_{MH} is the current state.

The mass balance for the solid hydride phase is given by:

$$(1-\varepsilon)\frac{d\rho_{MH}}{dt} = n_d \tag{11}$$

with ε denoting the effective porosity of the hydride bed.

The energy balance equation accounts for the thermal inertia of both the gas and solid phases and includes contributions from heat generated by the chemical reaction and heat exchanged via conduction and convection:

$$\left[\varepsilon\, \rho_g\, C_{p_g} + (1-\varepsilon)\, \rho_{MH}\, C_{p_{MH}}\right]\frac{\mathrm{d}T}{\mathrm{d}t} = \dot{Q}_{gen} + \dot{Q} \tag{12}$$

where C_{p_g} and $C_{p_{MH}}$ are the specific heat capacities of hydrogen and the hydride alloy, $\dot{Q}_{gen}$ is the thermal power associated with the reaction and $\dot{Q}$ is the net heat exchanged with the surroundings.
In particular, the reaction heat source term is defined as:

$$\dot{Q}_{gen} = -n_d \frac{\Delta H}{M_{H2}} \tag{13}$$

where ΔH is the enthalpy of reaction and M_{H2} the molar mass of hydrogen.

2.4. Numerical model

The system of governing equations described above was implemented in a MATLAB/Simulink R2023b model to simulate the dynamic behavior of the hydrogen storage tank during desorption and absorption; occasionally, some modifications have been adopted to make the model more suitable for representing absorption, such as the $f(p)$ term. Time integration of the resulting differential equations allows computing the evolution of hydrogen density in both the gas and solid phases, as well as the temperature profile across the system.

The internal volume of the tank was divided into multiple concentric domains: the metal hydride region (MH), the gas-filled porous region in contact with the alloy (lower H_2 domain) and the upper volume entirely occupied by hydrogen (upper H_2 domain). The steel wall of the tank (Tank domain) was modeled separately. A representative scheme of the discretization strategy is reported in Figure 2. The MH and lower H_2 domains were discretized radially into 50 nodes each, while the Tank domain was divided into 5 nodes; the upper H_2 domain was assumed to be homogeneous and was modeled using a single node, based on the assumption of uniform gas properties. The number of nodes in each domain was chosen by performing a sensitivity analysis on the model response to diverse hydrogen demand profiles: a trade-off criterion between accuracy and computational complexity was then used to determine the above numbers, making the model suitable for the integration into multi-physical complex systems, such as the microcar.
Each node represents a concentric cylindrical control volume. This geometric configuration allows computing heat fluxes between adjacent nodes by considering local thermal gradients and effective material properties. In the MH domain, these properties are evaluated as a porosity-weighted averages of the hydrogen and metal conductivities.

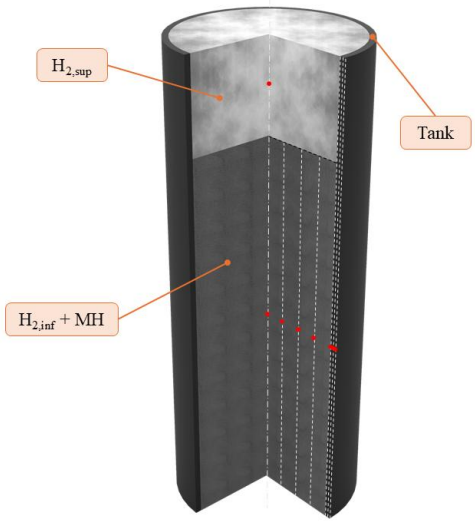

Figure 2. Domain discretization strategy adopted. Red dots represent the nodes position.

Concerning the thermal boundary conditions, they were applied to simulate different heat exchange configurations with the external environment. Convective heat transfer was implemented at the outer tank surface. Depending on the scenario, the model allows simulating a thermostatic bath with a fixed high convection coefficient, natural convection with ambient air, or forced convection induced by external airflow. All these conditions were formulated to modify the external heat flux term in the energy conservation equation, without altering the internal numerical structure of the model.

Thermal continuity was imposed at the interface between the MH and Tank domains, ensuring that the temperature at the transition node remained continuous and that the heat flux was correctly transferred across materials with different thermal properties.

Regarding initial conditions, the temperature of all nodes was set equal to the ambient temperature at the beginning of the simulation. The equilibrium pressure of the hydride material and the gaseous hydrogen pressure were defined to ensure thermodynamic consistency, enabling the calculation of the initial hydrogen concentration in the alloy through the PCI interpolation. This value was then used to estimate the initial hydride density.

2.5. Model validation

The model validation was conducted by comparing its results with those reported by Chung and Ho [19], who developed a 2D CFD model of a $LaNi_5$-based metal hydride tank, calibrated on the experimental data provided by Jemni *et al.* [18]. The experimental setup consisted of a sealed cylindrical vessel filled with hydride alloy and surrounded by a thermostatic bath at a fixed temperature. The PCI curves for $LaNi_5$ were digitized from [18] and interpolated using the rational third-degree equation (1). All physical and geometric parameters adopted for the simulation were taken from the work of Chung and Ho [19]. Compared to the implementation proposed by the present authors, the CFD-reference model also considered heat exchange through the bottom surface of the tank; given the comparable dimensions between the tank radius and the hydride bed height, small deviations are expected due to this additional heat transfer pathway.

The desorption process was simulated by initializing the system at thermal equilibrium with the external fluid, *i.e.* setting the initial temperature equal to the ambient value T_{ext} and assigning the corresponding equilibrium pressure p_{eq}. According to the simulation performed by Chung and Ho, the desorption process was divided into two subsequent phases: in the first 100 seconds, the external pressure p_{ext} was linearly decreased from p_{eq} to a target value p_{target}; in the second phase, p_{ext} was held constant at p_{target} to complete the hydrogen release.

Simulations were conducted by varying one of the two parameters (T_{ext} or p_{target}) while keeping the other fixed. The resulting hydrogen mass contained in the MH region during the desorption process was then computed and compared with the reference data. In one case, the external temperature was fixed at 313 K while the pressure target was varied; in the other, the target pressure was fixed at 1 bar and the temperature varied. The corresponding results are shown in Figure 3.

A slight deviation is visible in the profiles, especially for long time windows, which is likely due to simplifications adopted in the presented 1-D model with respect to the reference one, for example in the momentum formulation. Further investigations are planned to clarify this behavior. Additionally, the low values of m_{H_2} make the model extremely sensitive, where even slight mismatches with literature data lead to substantial relative errors.

To ensure consistency and clarity, the same validation procedure was applied to the absorption process, yielding the results presented in Figure 4.

Overall, the proposed model demonstrates robust predictive capabilities for both desorption and absorption phases, with results closely aligned with literature. Moreover, its accuracy is expected to improve further in configurations where radial dimensions are minor compared to

axial length, *i.e.* in tall and narrow tank geometries, where radial heat transfer dominates and axial contributions are negligible.

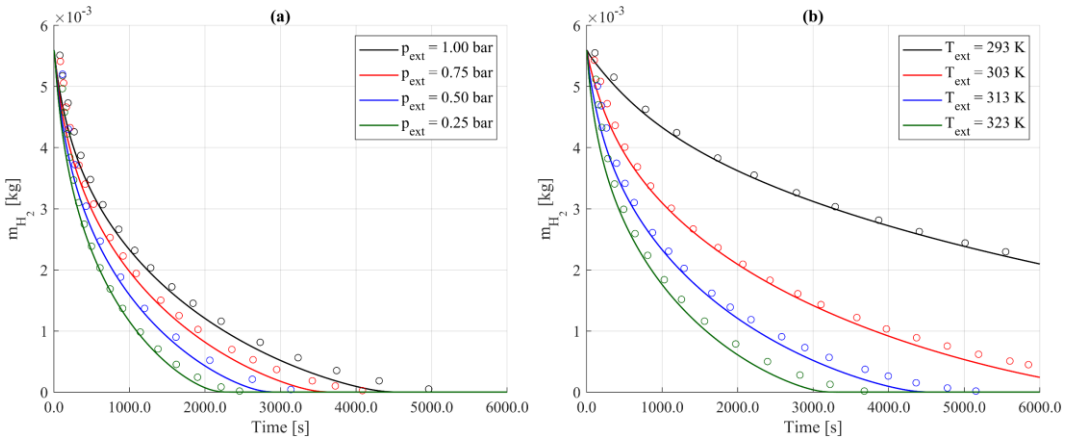

Figure 3. Total hydrogen mass in the MH region over time under varying boundary conditions, desorption case. (a) Constant temperature $T_{ext} = 313$ K, with different external pressures p_{ext}. (b) Constant pressure $p_{ext} = 1$ bar, with varying external temperatures T_{ext}. Circles represent reference data from Chung and Ho [19].

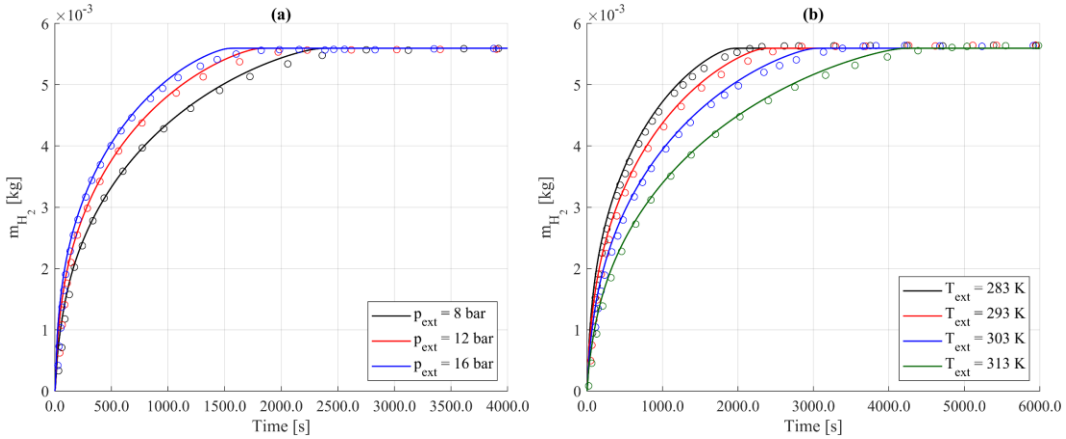

Figure 4. Total hydrogen mass in the MH region over time under varying boundary conditions, absorption case. (a) Constant temperature $T_{ext} = 313$ K, with different external pressures p_{ext}. (b) Constant pressure $p_{ext} = 1$ bar, with varying external temperatures T_{ext}. Circles represent reference data from Chung and Ho [19].

3. Results

The results presented in this section aim to evaluate the behavior of the proposed metal hydride storage system under realistic operating conditions. Simulations refer to a commercial AB_2-type alloy, Hydralloy C5, contained in the MyH2 3000 hydrogen storage tank manufactured by H2Planet, whose physical and geometrical properties are reported in Table 1.

As previously stated, one of the primary limitations of metal hydrides arises from their stringent thermal management requirements. Inadequate heat dissipation can lead to the interruption of hydrogen release. Therefore, to enable the practical implementation of such storage systems in real vehicles, it is essential to first assess the impact of different thermal management strategies on the behavior of the powder.

For this purpose, the analysis is divided into two parts. The first investigates the effect of various external thermal management techniques on the desorption process, in order to assess the viability of adopting passive heat management systems. The second evaluates the integration of the storage unit into a fuel cell hybrid electric microcar by simulating its performance over a representative driving cycle.

To evaluate the computational performance of the proposed model, computational and simulated times are reported in Table 2 for all the presented cases. The analysis has been carried out through a laptop equipped with an AMD Ryzen 7 6800H processor and a 64 GB DDR5 RAM. Both the solver and the variable timestep parameters were chosen automatically by the software. It is worth noting that the trade-off between model cost and detail makes it suitable for long-term simulations and implementation into complex system models.

Table 2. Execution and simulation times for thermal management strategies and seasonal operation with fuel cell integration.

Case	**Computational time [s]**	**Simulated time [s]**
	Thermal management effect (Section 3.1)	
Natural convection	6.65	7200
Forced convection	6.76	7200
High-efficiency thermal control	7.08	7200
	Seasonal impact with FC implementation (Section 3.2)	
Winter	253.86	1213
Spring	282.19	1213
Summer	271.51	1213
Autumn	282.38	1213

3.1. Effect of external thermal management

A series of simulations was conducted to investigate the impact of external thermal boundary conditions on the desorption behavior of the metal hydride storage system. Three scenarios were tested: natural convection with ambient air, forced convection representing fan-assisted cooling and an idealized high-efficiency case. While the latter is inspired by laboratory thermostatic bath setups, it is interpreted herein as a theoretical proxy for an advanced thermal management system, potentially realizable in optimized vehicular environments.

The system was subjected to an imposed outlet pressure of 2 bar and a constant hydrogen mass flow rate of $1.0 \cdot 10^{-5}$ kg $\cdot$ s^{-1}. The outlet pressure was selected in accordance with typical supply pressures of fuel cell stacks in automotive applications. The chosen flow rate was identified among various tested values as the most suitable to highlight the impact of different thermal boundary conditions applied to the storage system.

The hydride bed was initially assumed to be fully saturated with hydrogen and the initial pressure inside the tank was set equal to the equilibrium pressure corresponding to an ambient temperature of 293 K. The simulation covered a total duration of two hours.

In general, the desorption process, being strongly endothermic, is significantly affected by the low thermal conductivity of the metal hydride alloy, which limits the propagation of heat from the external environment to the relative core. As a result, a rapid drop in the temperature of the hydride occurs, leading to a corresponding decrease in the equilibrium pressure according to the van't Hoff relation. Therefore, the desorption reaction rate, governed by temperature, equilibrium pressure and gas pressure, progressively slows down until the equilibrium pressure equals the external pressure. At this point, the reactions ceases and hydrogen release is interrupted.

This phenomenon is sensitive to the efficiency of the external thermal exchange system. Figure 5 then shows the temperature evolution of the overall system over time for the proposed scenarios, under constant hydrogen demand.

In the case of natural convection, the rapid temperature drop leads the system to reach approximately −5 °C in about thirty minutes. This threshold corresponds to the condition where the equilibrium pressure of the hydrides decreases to 2 bar, matching the imposed outlet pressure, which in turn causes the desorption reaction to cease. When forced convection is applied, heat transfer from the environment to the tank is enhanced, resulting in a slower cooling rate. The critical condition is reached later than in the natural convection scenario, allowing the system to sustain hydrogen delivery for a longer period. Although the improvement is not as substantial as in the high-efficiency thermal control case, the temperature remains within a functional range for a more extended duration, thus improving the reaction stability. In contrast, the high-efficiency system maintains the alloy at higher and more stable temperatures throughout the simulation window, allowing continuous and uniform desorption.

These trends are reflected in Figure 6, which reports the hydrogen mass flow rates. Despite the constant demand imposed by the user, only the high-efficiency case can sustain the required desorption rate over time. The natural convection scenario exhibits an early drop in hydrogen supply, while forced convection results in intermediate performance: the system delays the shutdown of desorption and partially extends the duration over which the requested flow is met.

In conclusion, although the use of a high-efficiency thermal interface ensures the most favorable operating conditions, the adoption of a forced convection system offers substantial performance gains over natural convection (release time is almost doubled), with significantly lower complexity and energy requirements. Indeed, thermostatic-bath-idealized conceptualization requires ad-hoc design to meet compactness and weight vehicle requirements, while increasing total auxiliary energy demand. Conversely, easiness of realization makes passive heating an attractive and realistic option for the thermal management of metal hydride tanks in vehicular applications.

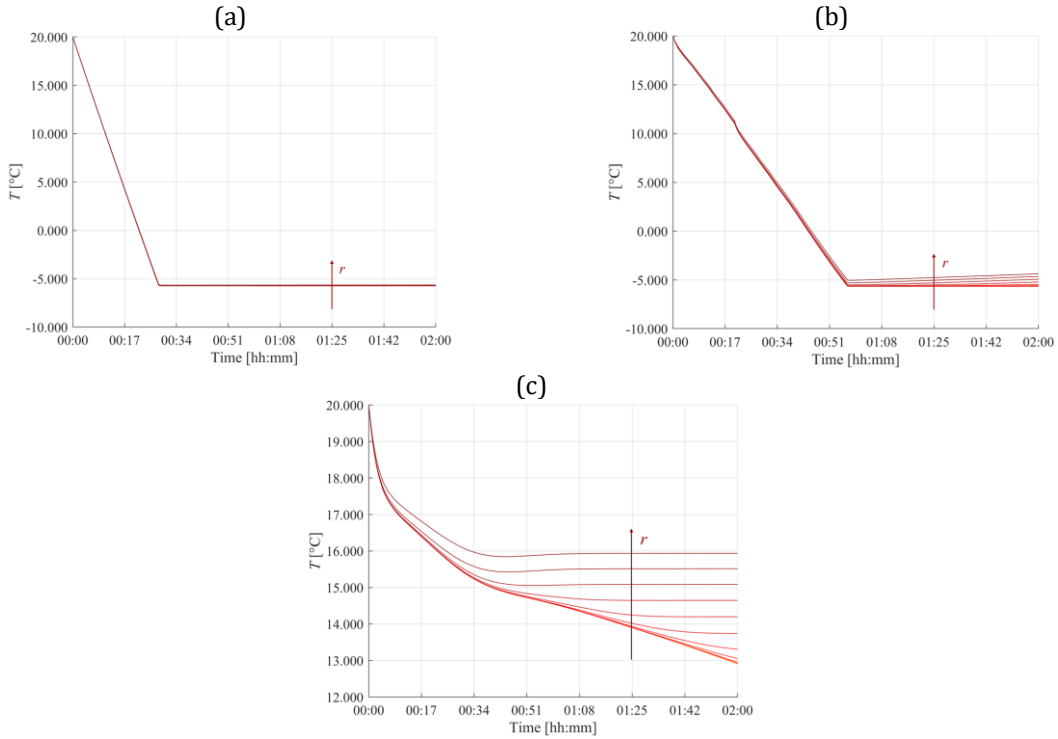

Figure 5. Temperature evolution of the hydrogen storage system under constant hydrogen demand; each line corresponds to a single node of the domain. (a) Natural convection, (b) forced convection, (c) high-efficiency thermal control.

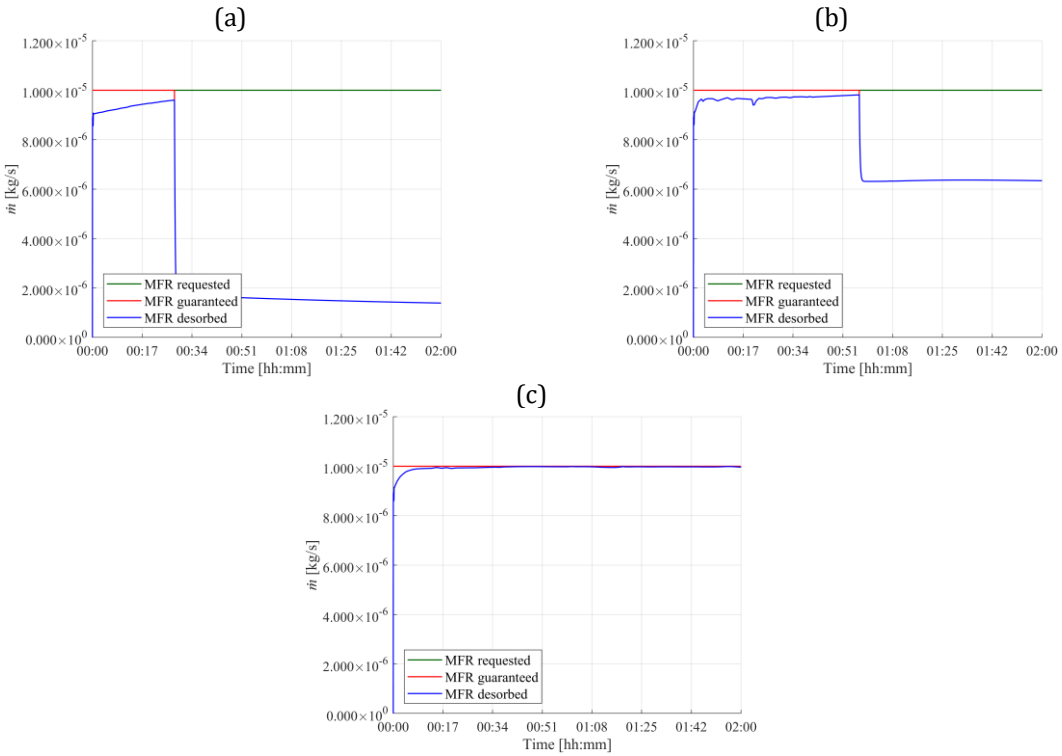

Figure 6. Hydrogen mass flow rates over time under constant demand. (a) Natural convection, (b) forced convection, (c) high-efficiency thermal control.

3.2. Integration with fuel cell system

Following the characterization of the fundamental desorption dynamics, the metal hydride storage system was coupled with a fuel cell unit to assess its performance under realistic operating conditions. The analysis focused on L6e-category light vehicles, where the adoption of active thermal management solutions is unfeasible due to complexity and cost constraints. For this reason, a passive strategy was considered, leveraging the warm airflow generated by the fuel cell stack itself.

Among several tests, a particularly relevant one is here reported, using the World Motorcycle Test Cycle (WMTC), which represents the homologation cycle with a standardized sequence of acceleration and deceleration patterns for reproducing a realistic drivability scenario. In a previous study, Bartolucci *et al.* [25] simulated the behavior of a PEM fuel cell (Horizon H2000) integrated into a hybrid microcar operating under WMTC conditions. The power demand profile obtained from the simulation, output of the simple fuzzy logic controller implemented, was used in a Hardware-in-the-Loop platform to extract the experimental hydrogen consumption curve, which includes both the stoichiometric flow required for the electrochemical reaction and periodic purge events characterized by sharp flow peaks.

The desorption behavior of the metal hydride system was then analyzed under the constraint of meeting this hydrogen demand. A configuration comprising two Hydralloy C5-based tanks in parallel was selected to reduce thermal stress on individual units and extend the overall release duration.

A key feature of this setup was the implementation of a passive forced convection system, similar to the one tested in the previous section: the exhaust airflow from the fuel cell blowers, normally used to supply reactant air and cool the stack, was redirected toward the storage tanks. The temperature of the airflow, assumed equal to the fuel cell stack temperature during the WMTC cycle, varies dynamically with the load and is consistently higher than the ambient temperature (around 45 °C), providing a valuable thermal input to the hydride beds. Based on an assumed outlet velocity of 5 $m \cdot s^{-1}$, a convective heat transfer coefficient of 25 $W \cdot m^{-2} \cdot K^{-1}$ was estimated using standard correlations for external airflow over a cylindrical geometry.

The simulation results, illustrated in Figure 7, demonstrate the effectiveness of this approach. The thermal contribution from the redirected airflow significantly reduces the temperature drop of the hydrides during desorption, thereby slowing the decrease in equilibrium pressure and maintaining favorable conditions for hydrogen release. As a result, the system is able to fulfill up to three WMTCs without interruption (Figure 7 (b)), a substantial improvement (75 %) compared to the case without thermal management (Figure 7 (a)), unable to complete the second cycle.

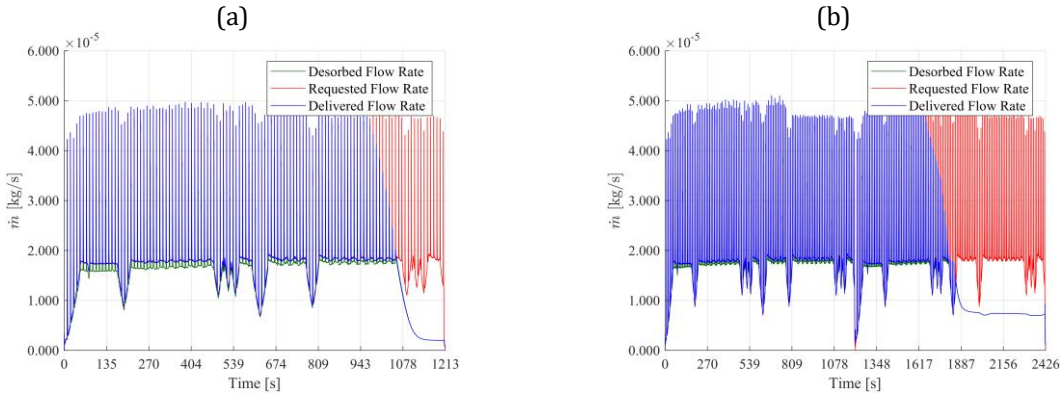

Figure 7. Hydrogen delivery performance under (a) natural convection and (b) forced convection. Desorbed flow rate (green) requested flow rate (red) and total delivered flow rate (blue) are shown. The forced-convection-based configuration ensures extended hydrogen availability and improved thermal response.

In fact, when compared to natural convection, where the thermal input is minimal and limited by the low convective coefficient of still air, the forced convection configuration yields a notably extended desorption duration and improved thermal uniformity. Under natural convection, the storage system tends to reach critical conditions much earlier. In contrast, the forced convection strategy not only delays the onset of such limitations but also ensures a more stable temperature profile throughout the tank, thereby enhancing the reliability and autonomy of the storage system.

To complement this evaluation, a seasonal analysis was carried out by repeating the same WMTC simulation under four representative ambient temperatures: 5 °C (winter), 15 °C (autumn), 20 °C (spring) and 30 °C (summer). In all cases, the same natural convection strategy was applied to better underscore the importance of environmental conditions. The results, reported in Figure 8, confirm a strong sensitivity of the storage system to external climate conditions. Lower ambient temperatures (Figure 8 (a)) worsen the cooling of the hydride material, accelerating the drop in equilibrium pressure and shortening the effective release period. Conversely, higher temperatures (Figure 8 (c)) enhance the thermal gradient with ambient air, improving heat exchange and sustaining desorption. Among the cases analyzed, only the summer condition (30 °C) allowed the system to complete over two WMTC cycles without interruption, while the winter scenario (5 °C) proved the most critical.

These results emphasize the importance of thermal boundary conditions and highlight the potential of passive forced convection as a practical solution to extend the usability of metal hydride storage systems. However, they also point to the need for additional design strategies – such as pre-heating or Phase Change Materials integration – and tailored control logics, to ensure consistent performance across different seasonal conditions. The combination of airflow reuse from the fuel cell provides a promising pathway for lightweight hydrogen-powered vehicles without relying on complex active subsystems.

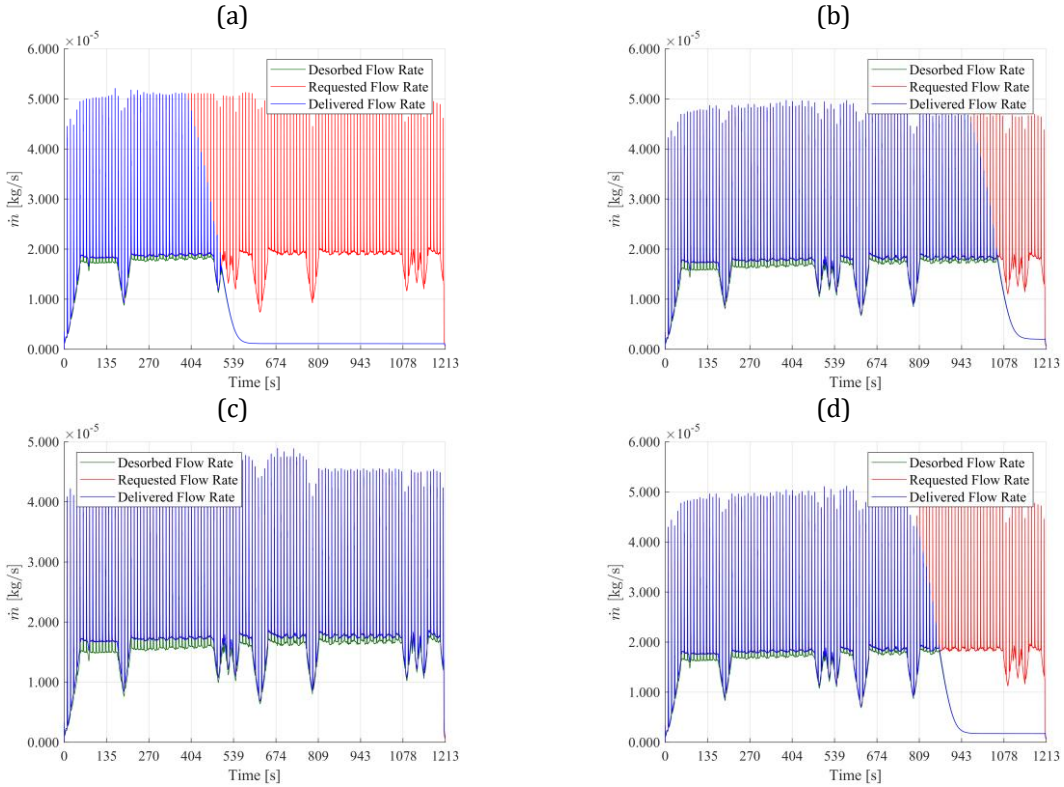

Figure 8. Effect of ambient temperature on the desorption process during WMTC cycles. (a) Winter case, with $T_{ext} = 5°C$; (b) Spring case, with $T_{ext} = 20°C$; (c) Summer case, with $T_{ext} = 30°C$; (d) Autumn case, with $T_{ext} = 15°C$.

4. Conclusions

The progressive decarbonization of the transport sector has increased interest in hydrogen as an alternative energy carrier for sustainable mobility. Among the possible applications, Fuel Cell Hybrid Electric Vehicles are receiving growing attention owing to their potential benefits in terms of autonomy and refueling time, making them an interesting complement to battery-based architectures. Nevertheless, storage remains one of the technical bottlenecks, especially in applications requiring compactness, safety and moderate operating pressures, such as microcars.

In this context, metal hydrides are being explored as an option for solid-state hydrogen storage, offering the advantage of reversible absorption and desorption processes at lower pressures than conventional high-pressure systems. However, the performance of these materials is linked to thermal boundary conditions, which must be carefully managed due to the thermochemical nature of the reactions involved: hydrogen absorption is exothermic and can lead to overheating, while desorption is endothermic and tends to induce progressive cooling, potentially inhibiting the release process over time.

To investigate these aspects, this study developed a numerical model capable of describing the thermofluid dynamic behavior of a Hydralloy C5-based storage tank under transient load conditions. The model incorporates thermodynamic and kinetic formulations and was validated against literature results. The platform was used to simulate different thermal management strategies and assess their influence on the system ability to meet hydrogen demand during operation.

The results indicate that the thermal management strategy significantly influences the system ability to support continuous hydrogen release. In particular, the use of a passive forced convection approach, based on redirecting the exhaust air from the fuel cell stack, was associated with a reduction in thermal gradients and slower cooling of the hydride bed; as a result, this contributed to maintaining equilibrium pressure and extending the duration of the desorption phase. Therefore, in FC-MH coupled simulations, this configuration enabled the system to cover multiple consecutive WMTC cycles without interruption, suggesting that this strategy could help improve reliability and operational range without introducing complex or energy-intensive subsystems.

Furthermore, the analysis conducted under different seasonal conditions highlighted the sensitivity of the storage system to ambient temperature. Lower external temperatures were associated with faster cooling and earlier desorption shutdown, whereas milder or higher temperatures facilitated more stable operation.

Overall, the proposed model and analysis framework may represent a useful tool for supporting the design and integration of solid-state hydrogen storage systems in fuel cell vehicles. Future developments may include experimental validation, the implementation of simplified control-oriented versions of the model and the investigation of system-level optimization strategies aimed at enhancing the coordination between the fuel cell stack and the storage unit.

References

[1]M. Ehsani, K. V. Singh, H. O. Bansal, and R. T. Mehrjardi, “State of the Art and Trends in Electric and Hybrid Electric Vehicles,” *Proc. IEEE*, vol. 109, no. 6, pp. 967–984, Jun. 2021, doi: 10.1109/JPROC.2021.3072788.

[2]J. Liu, F. Yang, Z. Wu, and Z. Zhang, “A review of thermal coupling system of fuel cell-metal hydride tank: Classification, control strategies, and prospect in distributed energy system,” *Int. J. Hydrog. Energy*, vol. 51, pp. 274–289, Jan. 2024, doi: 10.1016/j.ijhydene.2023.04.232.

[3]M. A. Aminudin, S. K. Kamarudin, B. H. Lim, E. H. Majilan, M. S. Masdar, and N. Shaari, “An overview: Current progress on hydrogen fuel cell vehicles,” *Int. J. Hydrog. Energy*, vol. 48, no. 11, pp. 4371–4388, Feb. 2023, doi: 10.1016/j.ijhydene.2022.10.156.

[4]A. Ewert, M. Brost, C. Eisenmann, and S. Stieler, "Small and Light Electric Vehicles: An Analysis of Feasible Transport Impacts and Opportunities for Improved Urban Land Use," *Sustainability*, vol. 12, no. 19, p. 8098, Oct. 2020, doi: 10.3390/su12198098.

[5]L. Bartolucci, E. Cennamo, S. Cordiner, M. Donnini, F. Grattarola, and V. Mulone, "Fuel Cell Hybrid Electric Vehicle: An Integrated Approach for Sub-Optimal Controller in Real-Time Application," presented at the WCX SAE World Congress Experience, Detroit, Michigan, United States, Apr. 2024, pp. 2024-01–2187. doi: 10.4271/2024-01-2187.

[6]L. Bartolucci, E. Cennamo, S. Cordiner, M. Donnini, F. Grattarola, and V. Mulone, "Fuel Cell Hybrid Electric Vehicle: Validated Fuel Cell and Battery Pack Model to Enhance Reliability in Performance Predictions," presented at the WCX SAE World Congress Experience, Detroit, Michigan, United States, Apr. 2024, pp. 2024-01–2188. doi: 10.4271/2024-01-2188.

[7]M. W. Davids *et al.*, "Metal hydride hydrogen storage tank for light fuel cell vehicle," *Int. J. Hydrog. Energy*, vol. 44, no. 55, pp. 29263–29272, Nov. 2019, doi: 10.1016/j.ijhydene.2019.01.227.

[8]L. Tribioli, G. Di Ilio, and E. Jannelli, "Fuel Cell/Battery Hybrid Lightweight Quadricycle with Metal Hydride Hydrogen Storage for Improved Performance," presented at the 16th International Conference on Engines & Vehicles, Capri, Italy, Aug. 2023, pp. 2023-24–0137. doi: 10.4271/2023-24-0137.

[9]D. J. Durbin and C. Malardier-Jugroot, "Review of hydrogen storage techniques for on board vehicle applications," *Int. J. Hydrog. Energy*, vol. 38, no. 34, pp. 14595–14617, Nov. 2013, doi: 10.1016/j.ijhydene.2013.07.058.

[10] L. Bartolucci and V. K. Krastev, "On the Thermal Integration of Metal Hydrides with Phase Change Materials: Numerical Simulation Developments towards Advanced Designs," presented at the Conference on Sustainable Mobility, Catania, Italy, Sep. 2022, pp. 2022-24–0018. doi: 10.4271/2022-24-0018.

[11] M. V. Lototskyy *et al.*, "Metal hydride hydrogen storage and supply systems for electric forklift with low-temperature proton exchange membrane fuel cell power module," *Int. J. Hydrog. Energy*, vol. 41, no. 31, pp. 13831–13842, Aug. 2016, doi: 10.1016/j.ijhydene.2016.01.148.

[12] G. Scarpati, E. Frasci, G. Di Ilio, and E. Jannelli, "A comprehensive review on metal hydrides-based hydrogen storage systems for mobile applications," *J. Energy Storage*, vol. 102, p. 113934, Nov. 2024, doi: 10.1016/j.est.2024.113934.

[13] P. Di Giorgio, G. Scarpati, G. Di Ilio, I. Arsie, and E. Jannelli, "Development of a plug-in fuel cell electric scooter with thermally integrated storage system based on hydrogen in metal hydrides and battery pack," *E3S Web Conf.*, vol. 334, p. 06013, 2022, doi: 10.1051/e3sconf/202233406013.

[14] G. L. Guizzi, M. Manno, and M. De Falco, "Hybrid fuel cell-based energy system with metal hydride hydrogen storage for small mobile applications," *Int. J. Hydrog. Energy*, vol. 34, no. 7, pp. 3112–3124, Apr. 2009, doi: 10.1016/j.ijhydene.2009.01.043.

[15] L. Bartolucci, E. Cennamo, S. Cordiner, M. Donnini, F. Grattarola, and V. Mulone, "A Hardware-in-the-Loop Platform for Developing a Fuel Cell Hybrid Electric Microcar: Fuel Cell Stack Sizing Using a Real-Time Testing Approach," presented at the Conference on Sustainable Mobility, Catania, Italy, Sep. 2024, pp. 2024-24–0006. doi: 10.4271/2024-24-0006.

[16] AMG Titanium - GfE Metalle und Materialien GmbH, "Hydralloy C Datasheet."

[17] h2planet, "MyH2 3000 - Cilindro per lo stoccaggio H2 in idruri metallici."

[18] A. Jemni, S. B. Nasrallah, and J. Lamloumi, "Experimental and theoretical study of a metal-hydrogen reactor".

[19] C. A. Chung and C.-J. Ho, "Thermal–fluid behavior of the hydriding and dehydriding processes in a metal hydride hydrogen storage canister," *Int. J. Hydrog. Energy*, vol. 34, no. 10, pp. 4351–4364, May 2009, doi: 10.1016/j.ijhydene.2009.03.028.

[20] M. Kölbig, I. Bürger, and M. Linder, "Thermal applications in vehicles using Hydralloy C5 in single and coupled metal hydride systems," *Appl. Energy*, vol. 287, p. 116534, Apr. 2021, doi: 10.1016/j.apenergy.2021.116534.

[21] T. Brown, J. Brouwer, G. Samuelsen, F. Holcomb, and J. King, "Accurate simplified dynamic model of a metal hydride tank," *Int. J. Hydrog. Energy*, vol. 33, no. 20, pp. 5596–5605, Oct. 2008, doi: 10.1016/j.ijhydene.2008.05.104.

[22] G. Capurso *et al.*, "Development of a modular room-temperature hydride storage system for vehicular applications," *Appl. Phys. A*, vol. 122, no. 3, p. 236, Mar. 2016, doi: 10.1007/s00339-016-9771-x.

[23] A. Hariyadi, S. Suwarno, R. V. Denys, J. B. Von Colbe, T. O. Sætre, and V. Yartys, "Modeling of the hydrogen sorption kinetics in an AB2 laves type metal hydride alloy," *J. Alloys Compd.*, vol. 893, p. 162135, Feb. 2022, doi: 10.1016/j.jallcom.2021.162135.

[24] S. Vyazovkin, A. K. Burnham, J. M. Criado, L. A. Pérez-Maqueda, C. Popescu, and N. Sbirrazzuoli, "ICTAC Kinetics Committee recommendations for performing kinetic computations on thermal analysis data," *Thermochim. Acta*, vol. 520, no. 1–2, pp. 1–19, Jun. 2011, doi: 10.1016/j.tca.2011.03.034.

[25] L. Bartolucci, E. Cennamo, S. Cordiner, M. Donnini, and V. Mulone, "Optimizing Hybrid Electric Microcar Design: A Simulation-Based Approach to Fuel-Cell Powertrains Analysis," *J. Phys. Conf. Ser.*, vol. 2893, no. 1, p. 012080, Nov. 2024, doi: 10.1088/1742-6596/2893/1/012080.